

Generation and processing of pseudo shear-wave data: Theory and case study

Vladimir Grechka* and Pawan Dewangan†

*Shell E&P, P.O.Box 481, Houston, TX 77001-0481

†Center for Wave Phenomena, Colorado School of Mines, Golden, CO 80401-1887

Summary

Processing of converted (PS) waves currently adopted by the exploration industry is essentially based on resorting PS data into common conversion point gathers and using them for velocity analysis. Here we explore an alternative procedure. Our key idea is to generate the so-called *pseudo-shear* (ΨS) seismograms from the recorded PP and PS traces and run conventional velocity analysis on the reconstructed ΨS data. This results in an effective S -wave velocity model because our method creates the data that possess kinematics of pure shear-wave primaries. Since we never deal with such complexities of converted waves as moveout asymmetry, reflection point dispersal, and polarity reversal, these generally troublesome features become irrelevant.

We describe the details of our methodology and apply the developed processing flow to a multicomponent ocean bottom cable line acquired in the Gulf of Mexico. Since the obtained stacking velocities of P - and ΨS -waves indicate the presence of effective anisotropy, we proceed with estimating a family of kinematically equivalent VTI (transversely isotropic with a vertical symmetry axis) velocity models of the subsurface.

Introduction

Due to a relatively high cost and poor quality of S -wave data excited on land and the absence of shear sources for marine surveys, PS -waves are often used to infer shear-wave velocities in the subsurface. Moveout of converted-waves, however, is usually asymmetric, which prevents one from applying conventional (e.g., hyperbolic) velocity-analysis methods to PS -waves. Processing of converted waves is further compounded by polarity reversal and reflection (or conversion) point dispersal – phenomena that are almost nonexistent for conventional P -waves. Recently, Grechka and Tsvankin (2002b) proposed a solution to the above outlined problems. Their $PP + PS = SS$ method uses traveltime picks of reflected PP and PS primaries from selected horizons to reconstruct traveltimes of the corresponding pure shear (SS) waves. Since the obtained S -wave moveouts are symmetric on CMP gathers, conventional velocity analysis can be applied to them. Implementation of the original, kinematic version of the method has two key elements: identifying PP and PS events reflected from the same interfaces and picking traveltimes from PP and PS prestack data (Grechka et al., 2002).

Here, we make the $PP + PS = SS$ method more practical. We describe a procedure that replaces the direct

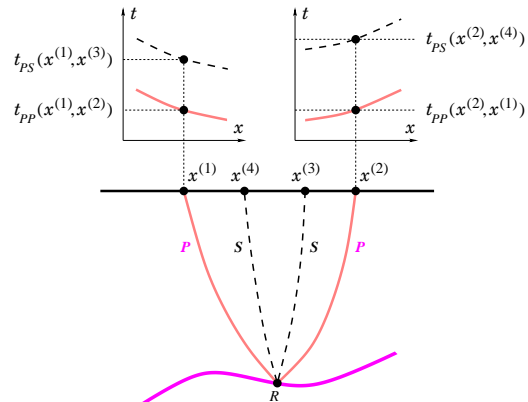


Fig. 1: Ray diagram of the $PP + PS = SS$ method in 2-D (after Grechka and Tsvankin, 2002b).

picking with a specially designed convolution of the original PP and PS traces. The result, which we call *pseudo-shear* (ΨS) data, has kinematics of pure- S primaries and, therefore, represents an appropriate input for conventional velocity analysis. We give the formulation of our procedure, explain why it works, and examine its performance on synthetic and field data. In particular, we demonstrate that our method is robust in the presence of random noise.

Application of our technique to a 2-D multicomponent line acquired in the Gulf of Mexico indicates anisotropy and, therefore, requires building of at least a VTI velocity model. Although the narrow-azimuth nature of the data and the absence of substantial dip leads to a family of kinematically equivalent subsurface models, we show that none of them is isotropic.

Kinematics of $PP + PS = SS$ method in 2-D

A natural point of departure for our development is kinematics of the $PP + PS = SS$ method. Figure 1 shows PP and PS ray trajectories that the method finds from 2-D split-spread PP and PS reflection data. Three rays $x^{(1)}R x^{(2)}$, $x^{(1)}R x^{(3)}$, and $x^{(2)}R x^{(4)}$ have exactly the same reflection point R if the pairs of PP and PS reflection slopes coincide at P -wave source and receiver locations. Then the geometry in Figure 1 produces pure- S reflected ray $x^{(3)}R x^{(4)}$. The traveltime t_{SS} along this ray is

$$t_{SS}(x^{(3)}, x^{(4)}) = t_{PS}(x^{(1)}, x^{(3)}) + t_{PS}(x^{(2)}, x^{(4)}) - t_{PP}(x^{(1)}, x^{(2)}), \quad (1)$$

where t_{PP} and t_{PS} denote the traveltimes of P - and

Generation and processing of ΨS -wave data

converted-waves, and $x^{(j)}$ ($j = 1, 2, 3, 4$) are the source and receiver coordinates.

Pseudo-shear traces

It turns out that direct traveltime picking can be replaced by computing the integral

$$w_{\Psi S}(t, x^{(3)}, x^{(4)}) = \iint \left[w_{PS}(t, x^{(1)}, x^{(3)}) * w_{PP}(-t, x^{(1)}, x^{(2)}) * w_{PS}(t, x^{(2)}, x^{(4)}) \right] dx^{(1)} dx^{(2)}. \quad (2)$$

Here w_{PP} and w_{PS} are the PP and PS seismic traces, t is time, and asterisks denote convolutions in time. The PP traces are taken in reverse time because the P -wave time gets subtracted in equation (1) to produce the pure-shear time. Integration is performed over P -wave source and receiver coordinates $x^{(1)}$ and $x^{(2)}$. The result of integration (2) is the ΨS trace for the source and receiver located at $x^{(3)}$ and $x^{(4)}$.

If the traces w_{PP} and w_{PS} consist of PP and PS primaries corresponding to a selected reflector, the trace $w_{\Psi S}$ contains the pure S -wave primary from the same reflector. This can be shown by transforming integral (2) into the frequency domain and applying the stationary phase method. Therefore, the correspondence of PP and PS events needs to be established and proper windowing of the input w_{PP} and w_{PS} traces has to be done prior to evaluating integral (2).

Synthetic examples

To demonstrate the performance of our method, we generated the PP and PS traces (Figures 2a and 2b) in a model containing three interfaces, windowed the events corresponding to the same reflectors, and computed integral (2). Figure 2c shows the reconstructed ΨS CMP gather. Note that our PP and PS data have the following features.

- PP and PS wavelets differ in both the shape and the frequency content; the ratio of dominant frequencies of PP - and PS -waves is 1.5.
- The polarity of reflected PS -waves flips at the zero offset.
- The converted-wave moveouts corresponding to dipping reflectors are asymmetric with respect to interchange of the source and receiver positions (Figure 2b). This phenomenon precludes applying conventional velocity analysis to PS data.

Figure 2c illustrates that the above features, which are usually troublesome for converted-wave processing, do not prevent us from obtaining meaningful ΨS data. The observation of primary importance in Figure 2c is that the ΨS events follow correct (i.e., computed by ray tracing) S -wave moveouts. The other features of ΨS are also worthwhile noting.

- As expected from the nature of convolution in equation (2), the ΨS wavelets are longer than either PP or PS ones. Their dominant frequency lies between those of

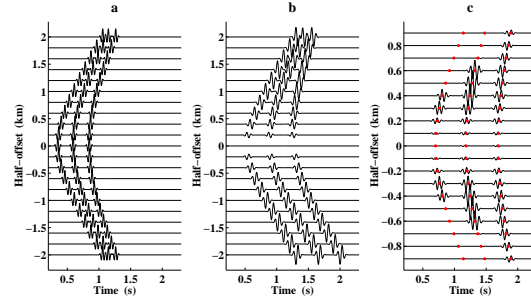


Fig. 2: Input (a) PP , (b) PS , and (c) generated ΨS CMP gathers computed for midpoint at the origin. The model is homogeneous and isotropic with $V_P = 4$ km/s and $V_S = 2$ km/s. Three planar reflectors have the depths $D = 0.7, 1.2,$ and 1.8 km beneath the origin; their dips are $0^\circ, 10^\circ,$ and 20° . Dots indicate correct S -wave reflection traveltimes.

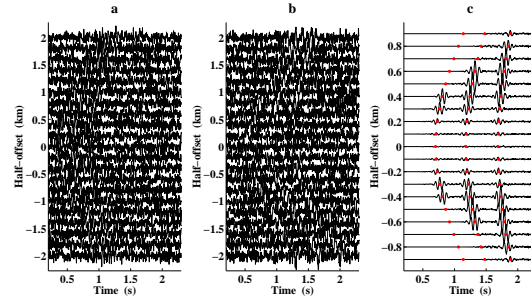


Fig. 3: Same as Figure 2 but for PP and PS data contaminated with Gaussian noise that has signal-to-noise ratio equal to 2. Dots indicate correct S -wave reflection traveltimes.

PP - and PS -waves.

- The ΨS CMP gather does not have polarity reversal. This follows from our formulation (2), which uses PS data twice so that the sign of PS polarity gets cancelled out.
- Weak amplitudes of ΨS -waves reconstructed at small offsets relate to the correspondingly weak PS signals. Clearly, the amplitudes of ΨS -waves are inherited from those of the PP and PS events. As a consequence, generating the ΨS data is *not* a true-amplitude procedure.
- The absence of ΨS -waves at large offsets is a result of limiting integration (2) to pre-critical offsets. They are equal to $X_{\Psi S}^{crit} = 2D \tan[\sin^{-1}(V_S/V_P)]$ for horizontal reflectors with depths D . In general, the ratio $X_{\Psi S}^{crit}/D$ is governed by the velocity ratio V_S/V_P . When V_S/V_P is small, the spreadlength of ΨS data might be insufficient for accurate S -wave velocity analysis.

Since we intend to apply the discussed procedure to field data, it is important to examine its robustness with respect to noise. Figures 3a and 3b show PP and PS traces similar to those in Figures 2a and 2b but contaminated with Gaussian noise that has standard deviation equal to 1/2 of the maximum amplitude of the signal. Even though the PP and PS reflections are hardly visible in Figures 3a and 3b, Figure 3c displays remarkably clean ΨS traces. Such a result is a direct consequence of applying convolutions, which efficiently attenuate random noise.

Generation and processing of ΨS -wave data

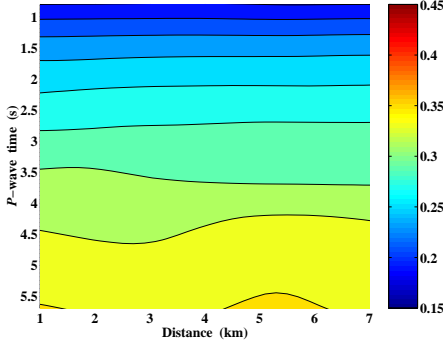


Fig. 4: Event correlation displayed as ratio g_0 [equation (3)]. The color bar refers to the values of and g_0 .

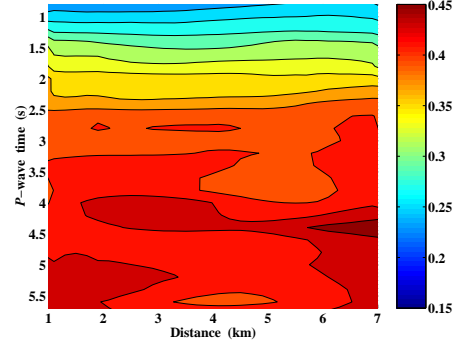


Fig. 6: Ratio $g_{nmo}(t_{PP0}, Y)$ of the picked ΨS - and P -wave NMO velocities. For comparison, the color scale in this figure is the same as that in Figure 4.

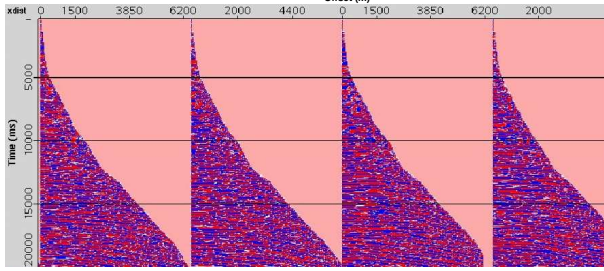


Fig. 5: Typical reconstructed ΨS CMP gathers.

Gulf of Mexico case study

We tested our methodology on a multicomponent (hydrophone, vertical geophone, and inline horizontal geophone) line acquired in the Gulf of Mexico. First, the PP -to- PS event correspondence was established. This gave us the relationship between PP and PS zero-offset times, t_{PP0} and t_{PS0} , which were used to compute the shear-wave traveltimes t_{SS0} and the ratios

$$g_0 \equiv \frac{t_{PP0}}{t_{SS0}} = \frac{t_{PP0}}{2t_{PS0} - t_{PP0}}. \quad (3)$$

Due to mild lateral heterogeneity, the function g_0 shown in Figure 4 displays a relatively weak dependence on the horizontal distance.

An important observation that can be made from Figure 4 is that the ratio g_0 is quite small (about 0.15) at shallow depths. If we ignore the possible presence of anisotropy, reflector dip, and lateral heterogeneity, and use the value of $g_0 = V_S/V_P = 0.15$ to estimate the critical ΨS offset-to-depth ratio, we find $X_{\Psi S}^{crit}/D \approx 0.3$. Clearly, shear-wave stacking velocities cannot be picked accurately from such short-spread moveouts. The ratio g_0 , however, rapidly increases as we go deeper, reaching the value of $g_0 = 0.35$ at t_{PP0} of around 5.5 s. This yields the ratio $X_{\Psi S}^{crit}/D \approx 0.75$ and makes the results of ΨS -wave velocity analysis substantially more accurate.

Figure 5, which displays the generated ΨS data, corrob-

orates the above observation. Indeed, we see a rapid increase of the maximum ΨS -wave offset as the time t_{SS0} (the vertical axis in Figure 5) grows. Velocity analysis performed on ΨS CMP gathers such as those in Figure 5 produces poorly resolved semblance maxima at shear times t_{SS0} smaller than about 5-6 s. This, however, is a consequence of low V_S/V_P ratio in the shallow layers rather than a deficiency of the applied procedure. The semblance maxima of ΨS -waves become better focused as t_{SS0} exceeds 6-7 s, which corresponds to P -wave times t_{PP0} between 2 and 3 s.

Evidence for effective anisotropy

Velocity analysis performed on ΨS CMP gathers (Figure 5) yields the S -wave normal-moveout (NMO) velocities $V_{S,nmo}$. Combining them with $V_{P,nmo}$ estimated from P -wave data, we find the effective ratio $g_{nmo} \equiv V_{S,nmo}/V_{P,nmo}$ (Figure 6). Comparison of g_{nmo} with g_0 (which is equal to the ratio of vertical velocities V_{S0}/V_{P0} if mild dips are ignored) shows that g_{nmo} is consistently greater than g_0 . For the P -wave times $t_{PP0} > 2.5$ s, where we expect the ΨS -wave NMO velocities to be sufficiently accurate, $g_0 \approx 0.3$ whereas $g_{nmo} \approx 0.4$.

As discussed by Grechka et al. (2002), only the presence of anisotropy can give plausible explanation for such a difference between the two velocity ratios. Therefore, the reconstructed subsurface model has to be anisotropic. Choosing the type of anisotropy to be VTI and assuming that horizontal inline geophones record SV -waves, we can construct the combination of g_0 and g_{nmo} ,

$$\frac{1}{2} \left(\frac{g_{nmo}^2}{g_0^2} - 1 \right) = \frac{\sigma - \delta}{1 + 2\delta} \equiv \chi, \quad (4)$$

that depends solely on Thomsen (1986) anisotropic coefficients δ and σ and, therefore, quantifies the effective anisotropy. The average values $g_0 \approx 0.3$ and $g_{nmo} \approx 0.4$ in Figures 4 and 6 yield $\chi \approx 0.4$ indicating that the subsurface is effectively anisotropic.

Generation and processing of ΨS -wave data

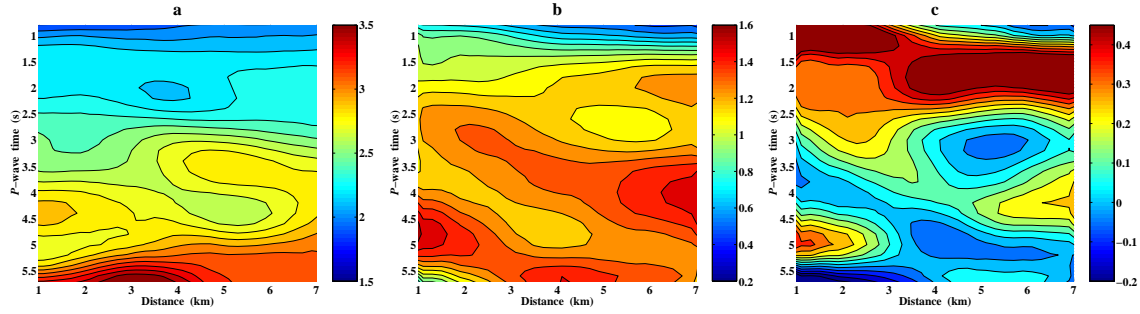


Fig. 7: Interval (a) P - and (b) ΨS -wave NMO velocities (in km/s), and (c) anisotropic coefficient χ .

Estimation of interval parameters

The feasibility of estimating anisotropy from reflection seismic data is governed by the amount of angular information that can be used in the inversion. Since the maximum absolute dip estimated from more than a thousand raw picks is less than 10° (the mean dip is about 2.5°), the subsurface can be treated as horizontally layered for the purpose of anisotropic inversion. As a consequence, the true depth cannot be estimated from reflected PP - and PS -waves even when long-spread data are available (Grechka and Tsvankin, 2002a). Therefore, we essentially have the following two choices. We can set either anisotropic coefficient δ or σ to any chosen constant value or any predetermined function and proceed with anisotropic stacking velocity tomography as was done by Grechka et al. (2002). The arbitrariness in δ or σ will produce a family of kinematically equivalent VTI depth models. Alternatively, we can perform parameter estimation in time domain that targets the interval NMO velocities $V_{P,nmo}$, $V_{S,nmo}$, and the coefficient χ treated as functions of the P -wave vertical time t_{PP0} . We select this option here.

Figure 7 displays our final output. Clearly, it hides significant depth ambiguity of the obtained VTI models. We still need to fix either anisotropic coefficient δ or σ to perform time-to-depth conversion. Neither of these coefficient, however, can be estimated from the data. Instead, the data constrain only their combination $\chi = (\sigma - \delta)/(1 + 2\delta)$ which does not allow us to resolve δ and σ individually; thus, the true depth remains unknown.

Discussion

We described the processing flow designed for velocity analysis of converted waves. Under the assumptions that (i) both PP and PS reflection data are available and (ii) the PP and PS event correspondence is established, we developed an automatic procedure for generating the ΨS data that ideally have kinematics of pure shear-wave primaries. As a result, conventional velocity analysis performed on ΨS CMP gathers yields S -wave NMO velocities. These velocities, along with those of the P -waves and the corresponding reflection dips, can be used for building elastic (usually anisotropic) interval-velocity models.

To construct the ΨS data, one has to integrate specially designed convolutions of PP and PS traces. We found that successful implementation of the technique requires selecting time gates that enforce the correspondence of PP and PS events and restricting the integration limits. One conclusion we drew along the way was that the spread of ΨS data is always limited by the critical offset. Although this result directly follows from Snell's law, it has the following important practical implication: small S - to P -wave velocity ratios always produce ΨS CMP gathers that have insufficient spread for accurate shear-wave velocity analysis.

We tested our methodology on both synthetic and field data. While synthetic examples helped us to establish some data requirements and characteristics (e.g., PP and PS wavelets do not have to be the same, random noise is not a problem), the presented case study demonstrated that our processing flow produces results useful for building anisotropic velocity models of the subsurface.

We have left a few issues almost completely undeveloped. A potential research area lies in making use of ΨS -wave AVO behavior to extract the PS AVO signature. An apparent advantage of dealing with ΨS rather than with PS data includes simpler moveouts and usually higher signal-to-noise ratio of the former. Generating ΨS -waves and estimating shear-wave velocities also provides solid ground for migration of ΨS data. Since this has not been done so far, it remains to be seen what can be gained from the ΨS images.

References

- Grechka, V., and Tsvankin, I., 2002a, The joint nonhyperbolic moveout inversion of PP and PS data in VTI media: *Geophysics*, **67**, 1929–1932.
- Grechka, V., and Tsvankin, I., 2002b, $PP + PS = SS$: *Geophysics*, **67**, 1961–1971.
- Grechka, V., Tsvankin, I., Bakulin, A., Hansen, J.O., and Signer, C., 2002, Joint inversion of PP and PS reflection data for VTI media: A North Sea case study: *Geophysics*, **67**, 1382–1395.
- Thomsen, L., 1986, Weak elastic anisotropy: *Geophysics*, **51**, 1954–1966.